In Proceedings of the IEEE International Conference on Robotics and Automation (ICRA 2013), May 6-10, 2013, Karlsruhe, Germany. (In Press)

# Needle Path Planning for Autonomous Robotic Surgical Suturing

Russell C. Jackson and M. Cenk Çavuşoğlu

*Abstract*— **This paper develops a path plan for suture needles used with solid tissue volumes in endoscopic surgery. The path trajectory is based on the best practices that are used by surgeons. The path attempts to minimize the interaction forces between the tissue and the needle. Using surgical guides as a basis, two different techniques for driving a suture needle are developed. The two techniques are compared in hardware experiments by robotically driving the suture needle using both of the motion plans.**

## I. Introduction

Even with the help of robotic surgical systems, suturing is a challenging and time consuming task during Minimally Invasive Surgery (MIS). Automating the suturing task may reduce both the time and difficulty of completing a suture. Pre-planning the autonomous motion, when combined with force feedback, would allow the robot to minimize any tissue trauma that might occur during suturing. Well established manual suture techniques lay the foundation for robotic suturing. In order to complete an independent surgical suture, several components must be preplanned. First, the needle must enter and exit the tissue in the proper locations and orientations. Secondly, the needle path must not put any unnecessary stress on the tissue. Finally, the needle must be able to react to any unforeseen obstacles that might impede the needle's path.

In an earlier study, Nageotte et al. [9] presents a path planning method for a laparoscopic suture needle through tissue membranes using a limited degree of freedom laparoscopic instrument. This is different than suturing a solid block of tissue together. When the needle is penetrating the membrane surface, stress only occurs at the site of needle penetration. When a solid volume of tissue is sutured, the entire embedded needle body may be deforming the tissue. Advances in MIS, (e.g. the daVinci® system built by Intuitive Surgical based in Sunnyvale California) also grant additional dexterity to the needle driver. The additional degrees of freedom enable the suture plan to be optimized for patient care quality.

There are also earlier studies on planning algorithms for percutaneous needle insertion, such as for biopsy, brachytherapy, etc (e.g. [3], [5], [2]). In percutaneous interventions, long and flexible needles are used to reach targets embedded deep inside the tissue. As such, the methods and algorithms developed for these applications cannot be applied to the planning of surgical suturing.

The goal of this paper is to create, using the best practices of manual suturing, a path for suturing with a semi-circular needle. Section II lays the groundwork for the needle plan using both the surgeons' best practices and their mathematical analogs. This is followed in section III with a step by step needle trajectory. The needle trajectory has two potential approaches. The two versions are empirically tested in section IV. The results of the two needle drives are analysed in section V. The paper concludes with a discussion of planned future work.

## II. Best Practices of Suturing

There are many general rules that surgeons use to complete a suture. A typical list of such rules is below [10] [11]. Manual needle sutures normally result in a picture similar to Fig. 1.

1. The needle first "bites" the tissue orthogonally. By inserting the needle such that the tip is orthogonal to the tissue surface, tissue surface stress is minimized.
2. The wrench between the tissue and the needle during the suture must be minimized. Minimizing the needle tissue interaction force reduces the internal tissue stress, and consequently reduces additional tissue trauma due to the suture.
3. The re-grippable length of the needle during the suture must be adequate for the needle re-grasp to be completed successfully. Since the needle holder can not be inserted through the tissue, there must be an intermediate point during the suture that the gripper can regrasp the needle on the tip to complete the suture.
4. The final depth of the needle in the tissue is an important component of a successful suture. The actual target depth is determined by many factors, including both the wound being closed and the size of the needle.
5. The needle tip should only touch the tissue at the insertion site. Similarly, the needle gripper should not place unnecessary stress on the tissue.

The above list is not exhaustive, but details important components of a quality suture.

Converting the listed suture principles into a list of analytic equations allows for the planning algorithm to be automated and optimized against the suture guidelines.

### A. Quantification of the Suturing Guidelines

The principles above can be adapted to equations directly. The bite angle of the needle is measured using the initial needle insertion vector. This unit vector ($\boldsymbol{k}$) is shown in Fig.

This work was supported in part by NSF under grants IIS-0805495, IIS-0905344, and CNS-1035602, and National Institutes of Health under grant R21 HL096941.

The authors are with the department of Electrical Engineering and Computer Science (EECS) at Case Western Reserve University in Cleveland, OH. The corresponding author M. Cenk Çavuşoğlu can be reached at cavusoglu@case.edu

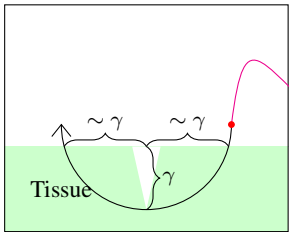


Fig. 1: This is an example image of a suture (adapted from [11]). Once the needle completes the suture, the suture thread (purple) will close the wound (triangle cut out of the tissue). The distance of the entry point and the exit point from the wound are approximately equal to the depth of the needle ($\gamma$). The tip of the needle is the arrow. The base of the needle is marked by a circle. To avoid clutter, the thread will be absent from other needle figures.

2. The local tissue normal vector is $\boldsymbol{y}_0$. The inner product between the needle tip $\boldsymbol{k}$ and $\boldsymbol{y}_0$ approaches $-1$ as the needle tip penetrates the tissue orthogonally. Since best practices of suturing call for an orthogonal tissue bite, defining a metric $b = -\boldsymbol{k}^T\boldsymbol{y}_0$ is one method of assessing the quality of the needle insertion. After evaluating the initial insertion angle of the needle, the next task is to critique the interaction forces felt by the needle during the suture. Minimizing the forces and torques that act between the needle and the tissue can be posed in multiple ways. The first method is to minimize the maximum forces and torques between the tissue and the needle during the suture. Another technique is to minimize the average forces and torques. Modeling the tissue-needle forces during the planning stage will improve the overall quality of the needle plan. While many different tissue needle force models exist [1], a fast force and torque model of the suture needle tissue interaction is developed in [6]. This force torque model includes three components. The first one is a friction force that acts tangentially to the needle. The second one is a tissue deformation force that acts normal to the needle. The final force is due to the cutting of the tissue. The cutting force acts exclusively on the needle tip.

In order to regrasp the needle during the suture, there must be a point during the suture such that the exposed needle tip can be gripped. Simultaneously, the gripper holding the needle base must deform the tissue as little as possible. One way of determining this is to calculate the amount of needle exposed during the regrasping stage.

The final depth of the needle in the tissue could be calculated by using the distance between the entrance $\boldsymbol{g}$ and the exit $\boldsymbol{f}$. The depth of the needle is derived using the following set of equations. Figure 3 illustrates the geometry that is used to derive the equations. The distance between the points $\boldsymbol{f}$ and $\boldsymbol{g}$ is $p$. The quantity, $p$, coupled with the needle radius, $r$, allows the height, $h$, of the $\boldsymbol{gcf}$ triangle to be calculated as:

$$h = \sqrt{r^2 - (p/2)^2}. \tag{1}$$

The maximum depth of the needle, $d = h - r$, can then be calculated. The ideal depth of the needle varies based on the application [11].

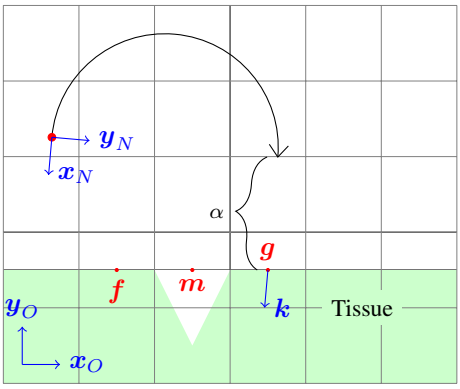


Fig. 2: This is the pose of the needle before it begin to bite the tissue. Notice that the tip of the needle is nearly but not quite orthogonal to the tissue. The scaler $\alpha$ is the initial distance between the needle tip and the needle entrance point. $\boldsymbol{m}$ is the location of the tissue break undergoing repairs. Ideally $\boldsymbol{m}$ is midway between $\boldsymbol{g}$ and $\boldsymbol{f}$. The location defined by $\boldsymbol{f}$ is the point where the needle is supposed to exit the tissue.

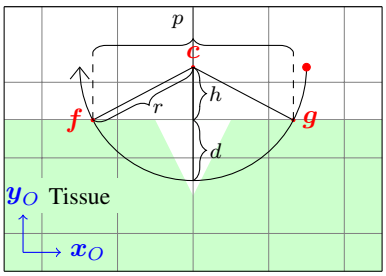


Fig. 3: The depth of the needle in the tissue ($d$) can be calculated using the distance ($p$) between the needle entrance ($\boldsymbol{g}$) and exit ($\boldsymbol{f}$) points along with the needle radius ($r$). The values $p$ and $r$ in turn generate the height of the needle center ($\boldsymbol{c}$) above the tissue. This value is given by $h$. The difference between $r$ and $h$ gives the needle depth in the tissue.

The final constraint is that during the initial insertion, the needle base cannot touch the tissue. Likewise during needle extraction, the needle tip should not reinsert into the tissue. Due to the potential complications associated with either of the above cases, any path plan that causes the needle base to touch the tissue or the needle tip to reinsert into the tissue should be readily rejected as a viable candidate.

## III. Needle Path Planning Algorithm

For the purposes of planning the path, assumptions about both the needle and tissue geometry are made. The tissue volume is locally approximated as a rectangular prism, while the needle is approximated as a semi circle. The needles being used are sold as 1/2 circle needles. The needle path itself can be broken down into 5 distinct components: needle approach, initial needle insertion, needle reorientation, needle regrasp, and finally, needle follow through. The needle approach is where the needle moves into a position that is near

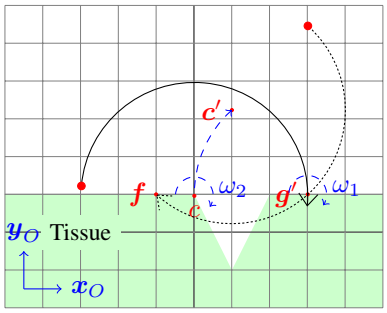


Fig. 4: Once the needle has penetrated the tissue, it is now possible to reorient the needle so that the needle will naturally drive to the target exit point. The point $\boldsymbol{f}$ is the location of the exit point. The dashed view of the needle is a sample orientation of needle after completing the alignment. The point $\boldsymbol{c}$ is the point that the needle center starts at. After the needle finishes the alignment, the center of the needle is now at $\boldsymbol{c}'$. The dashed curve from $\boldsymbol{c}$ to $\boldsymbol{c}'$ is the curve that the center of the needle will move through. Notice that this curve is a circular arc that is centered on the point $\boldsymbol{g}'$. The scalar, $\omega_1$, is the angular rate of rotation of the point $c$ about $\boldsymbol{g}'$. The angular velocity $\omega_2$ is the speed of rotation of the body of the needle about the center point $c$.

the tissue and properly oriented for the needle bite. During the needle bite, the needle penetrates the tissue until the needle has reached a target depth. Once the initial insertion is complete, the needle is pushed forward through the tissue while reorienting. The reorientation is required so that the needle will exit the tissue at the correct point. After finishing the reorientation, the needle completes the suture by moving the tip in the same circle defined by the arc of its body. Either during the needle reorientation or the needle follow through, the needle tip will egress from the tissue. When the needle tip is exposed, the gripper can grasp the tip and complete the suture. Once the regrasp is complete, the needle should only move in an ideal circular path. This minimizes tissue stress for the remainder of the suture. The motion plan is centered about the needle for convenience.

### A. Needle Approach

The needle approach is shown in Fig. 2. The information needed to generate the initial approach pose include the points $\boldsymbol{g}$ and $\boldsymbol{f}$, the vector $\boldsymbol{k}$, and the initial insertion distance $\alpha$. The quantities are all used to define the initial needle position. The intersecting vectors $\boldsymbol{k}$ and $\boldsymbol{f}-\boldsymbol{g}$ uniquely define a plane. The semi-circular needle lies in this plane. The vector $\boldsymbol{k}$, points along the needle tip. This combined with the plane of the needle completely defines the needle orientation. This orientation can be described as a matrix, $R_{ON} \in \mathrm{SO}(3)$. The scalar $\alpha$ defines the initial starting distance between the needle tip and the point $\boldsymbol{g}$. The position and orientation of the needle can be represented using $g_{ON} \in \mathbb{R}^{4\times4}$. The matrix, $g_{ON}$, represents a homogeneous transformation from the needle frame $(N)$ to the tissue frame $(O)$ in $\mathrm{SE}(3)$. This homogenous transform is uniquely defined by $R_{ON}$ and $\boldsymbol{p}_{ON} \in \mathbb{R}^{3\times1}$. The vector $\boldsymbol{p}_{ON}$ is defined using the initial bite angle $\alpha$:

$$\boldsymbol{p}_{ON} = \boldsymbol{g} - \alpha\boldsymbol{k} - 2r\boldsymbol{y}_N \tag{2}$$

### B. Needle Bite

Once the needle is in position (Fig. 2), the suture is started. This is done by moving the needle along the tip vector ($\boldsymbol{k}$) until it has penetrated the point $\boldsymbol{g}$ to a predetermined depth. This depth ($\beta$) comprises one of the inputs to the overall suture plan. The depth determines both the amount of deformation that the tissue may undergo as well as the amount of needle grip in the tissue. If the needle is not inserted deep enough, the tip may only skip along the surface as it reorients. If the needle is too deep, then the needle reorientation may cause too much displacement of the tissue. During the bite, the needle moves with the body velocity,

$$\boldsymbol{V}^b_{ON} = \begin{bmatrix}1 & 0 & 0 & 0 & 0 & 0\end{bmatrix}^T. \tag{3}$$

The body velocity can be scaled. Increasing the speed will decrease the suture time, decreasing the speed will result in a gentler needle insertion.

### C. Needle Reorientation

Once the needle has penetrated the tissue, the needle is reoriented so that it will egress at the correct point on the opposite side of the wound. The reoriented center point of the needle is calculated using the available geometric information. The actual needle intersection point can be computed by starting with the actual needle height,

$$h' = \boldsymbol{y}_0^T(\boldsymbol{c} - \boldsymbol{g}), \tag{4}$$

where $\boldsymbol{c}$ is the needle center, and $h'$ is distance from the tissue surface to the needle center. The point $\boldsymbol{m}$ is the location of the wound undergoing suture. The point on the tissue surface closest to the current center of the needle, $\boldsymbol{m}'$, is

$$\boldsymbol{m}' = \boldsymbol{c} - (h')\boldsymbol{y}_0. \tag{5}$$

The orthogonal projection of the needle basis vector $\boldsymbol{y}_n$ on the tissue normal $\boldsymbol{y}_0$ is defined as $\boldsymbol{y}'_n$. The point where the needle actually intersects the tissue, $\boldsymbol{g}'$, ($\boldsymbol{g} \neq \boldsymbol{g}'$ due to the curve of the needle) can be computed as

$$\boldsymbol{g}' = \boldsymbol{m}' + \boldsymbol{y}'_n\sqrt{r^2 - h'^2}. \tag{6}$$

Once the actual needle entrance point, $\boldsymbol{g}'$ is found, the target exit point $\boldsymbol{f}$ is used to compute the target needle center location $\boldsymbol{c}'$. The midpoint between $\boldsymbol{g}'$ and $\boldsymbol{f}$ is given as $\boldsymbol{p}_m$. The distance $p' = \|(\boldsymbol{f} - \boldsymbol{g}')\|$ allows the new target center of the needle, $\boldsymbol{c}'$, to be computed as

$$\boldsymbol{c}' = \boldsymbol{y}_0\sqrt{r^2 - (p'/2)^2} + \boldsymbol{p}_m. \tag{7}$$

Once the target center position of the needle is defined, there are multiple ways to reorient the needle. One such method is to use a "static point". The static point is where the needle does not move in a way that deforms the tissue. This point is the fulcrum that the needle center moves around. Selecting a "static point" that minimizes the overall tissue

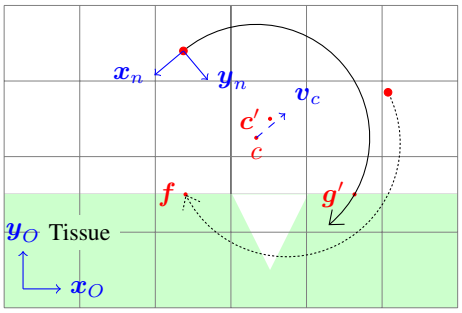


Fig. 5: The non holonomic motion plan reorients the needle such that the tip velocity is exclusively tangential. The vector, $\boldsymbol{v}_c$, is the motion of the needle center, $\boldsymbol{c}$, towards the desired needle center, $\boldsymbol{c}'$. Since $\boldsymbol{v}_c$ is parallel to $\boldsymbol{x}_n$, it is not pointed directly at the target, $\boldsymbol{c}'$.The dashed line representing the needle is one possible position of the needle after reaching the exit, $\boldsymbol{f}$. Notice that the new needle position no longer passes through the point $\boldsymbol{g}'$. This is due to the fact that the invariant motion of $\boldsymbol{g}'$ must be sacrificed to maintain the non holonomic motion constraint.

trauma (e.g minimize the forces and torques) would be the optimal point of rotation. Another method of reorienting the needle is to drive the tip such that it can only go forward along the tangent direction or rotate about the tip point. The goal of the non holonomic constraint is to avoid having the needle tip tear laterally through the tissue during the suture. A feature common to both types of needle reorientation is that the needle tip is always moving forward through the tissue.

*1) Needle Reorientation About The Entrance Point:* In this case, the rotation is computed about the site where the needle penetrates the tissue. This is done to avoid stress on the point of needle penetration. Fig. 4 shows the needle as it realigns from the bite position to the follow through pose. During the reorientation, the needle center moves in a circle about the point $\boldsymbol{g}'$ with an angular speed of $\omega_1$. Simultaneously, the needle is rotating about its center $\boldsymbol{c}$ with an angular rate of $\omega_2$. The needle frame velocity is sum of the two components. The component due to the rotation about the needle entrance, $\boldsymbol{g}'$, is calculated using the transform $g_{ON}$. The vector $\boldsymbol{p}$ is the vector that points from the point $\boldsymbol{g}'$ to the center of the needle ($\boldsymbol{c}$), as measured in needle coordinates. This vector is then used to create the body velocity component required to spin the needle about its current insertion point.

$$\begin{bmatrix}\boldsymbol{p}\\0\end{bmatrix} = g_{ON}^{-1}\left(\begin{bmatrix}\boldsymbol{c}\\1\end{bmatrix} - \begin{bmatrix}\boldsymbol{g}'\\1\end{bmatrix}\right) \tag{8}$$

$$\begin{aligned}\boldsymbol{V}_{ON}^{b} &= \omega_2\begin{bmatrix}-2r & 0 & 0 & 0 & 0 & -1\end{bmatrix}^2 \\ &+\omega_1\begin{bmatrix}\boldsymbol{p}^T \times \begin{bmatrix}0 & 0 & -1\end{bmatrix} & 0 & 0 & -1\end{bmatrix}^T\end{aligned} \tag{9}$$

*2) Non-Holonomic Needle Rotation:* When driving the needle such that the tip velocity is tangent to the tip, the velocity of the needle center must also be tangent to the tip vector. The difference between the center of the needle, $\boldsymbol{c}$, and the new target center, $\boldsymbol{c}'$, (as given by eq. 7) is the position error of the center. The velocity is then computed to be proportional of the alignment between $\boldsymbol{e_c}$ and $\boldsymbol{x}_n$.

$$\boldsymbol{e_c} = \boldsymbol{c} - \boldsymbol{c}' \tag{10}$$

$$\boldsymbol{V_c} = \boldsymbol{e_c}(\boldsymbol{x}_n^T\boldsymbol{e_c}) \tag{11}$$

$$= \begin{bmatrix}-r\omega_1 & 0 & 0\end{bmatrix}^T \tag{12}$$

The overall equation of motion is then generated as follows:

$$\begin{aligned}\boldsymbol{V}_{ON}^{b} &= \omega_2\begin{bmatrix}-2r & 0 & 0 & 0 & 0 & -1\end{bmatrix}^T \\ &+\omega_1\begin{bmatrix}-r & 0 & 0 & 0 & 0 & -1\end{bmatrix}^T.\end{aligned} \tag{13}$$

When moving the needle non holonomically, the rest of the needle has to sweep a large arc to keep the tip moving tangentally. This results in larger needle tissue deformations. This also constraints the velocity of the needle center, $\boldsymbol{c}$, to be tangent to the circle about the needle tip. This is shown in Fig. 5.

A stop motion time lapse comparison between the two proposed motion styles is shown in Fig. 6a and 6b. The holonomic motion plan does appear to have some tearing due to the needle tip moving sideways. The non holonomic motion plan appears to sweep out a much larger area, but does not appear to cause tissue tearing at the needle tip. Directly modeling these effects on the tissue is outside of the scope of this paper.

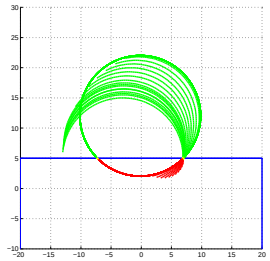

(a) Time lapse of the holonomic needle motion.

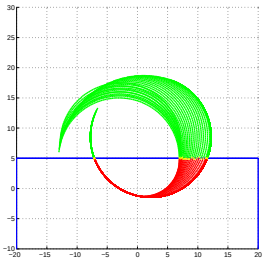

(b) Time lapse of the non holonomic needle motion.

Fig. 6: The images above are composite images of the needle position as it moves. The needles are colored green, yellow, and red. The green portion corresponds to the portion of the needle outside the tissue. The yellow portion is where the needle enters the tissue. Finally, the needle is colored red inside the tissue. The two different reorientations have different overall effects on the tissue. In Fig. 6a, the needle sweeps out a small area during the reorientation, but there is no area swept at the point where the needle intersects the tissue. In Fig. 6b, tissue stress at the needle tip is minimized, but the needle sweeps out a larger area. It also appears that the needle is deeper inside the tissue for the non holonomic needle motion.

### D. Needle Regrasping

Once the needle completes the reorientation, it begins the needle follow through. Once the needle tip penetrates

TABLE I: Variable Inputs Required for Needle Plan

| Input | Description |
|---|---|
| $\boldsymbol{g}$ | The needle bite target |
| $\boldsymbol{k}$ | The needle bite direction |
| $\boldsymbol{f}$ | The needle exit point |
| $\alpha$ | The initial approach distance |
| $\beta$ | The initial needle bite depth |
| $\omega_1$ | The angular speed of reorienting the needle |
| $\omega_2$ | The angular speed of driving the needle |

the tissue, even if it is before reorientation is complete, the needle is regrasped and extracted to prevent excessive distortion of both the entrance and egress point of the needle. During the regrasp, the gripper can be oriented to optimize its dexterity for future steps. After regrasping, no further reorientation is attempted because the needle tip is already poking out of the tissue. Any attempt to reorient at this point will only serve to stress the tissue further. In order for the regrasp to be reliable, it will be important to incorporate visual servoing to assist the robot in regrasping the needle [4].

### *E. Needle Follow Through*

Once the needle has been aligned or regrapsed, the needle will be moved while minimize its tissue deformation. This is accomplished by imposing the following body velocity on the needle

$$\boldsymbol{V}_{ON}^{b} = \omega_2 \begin{bmatrix} -r & 0 & 0 & 0 & 0 & -1 \end{bmatrix}^T. \qquad (14)$$

By moving the needle along its own arc, further tissue distortion is minimized.

### *F. Needle Path Input List*

The primary inputs required to generate the needle path plan are listed in Table I. The first four inputs are used for the needle approach and set up. The final three parameters are used for the needle drive itself. The parameters $\omega_1$ and $\omega_2$ are used in both holonomic and non holonomic needle drives.

## IV. Empirical Path Evaluation

In this section, experimental validation of the proposed method for generating the needle path is presented. Since there are two potential methods of generating the needle path, it is important to understand the practical differences between them during actual needle sutures. To compare the two flavors of the needle drive, a suture needle was driven through a test sample of a tissue phantom. The robot driving the needle is a novel laparoscopic gripper [7] with an embedded force sensor attached to a ABB IRB140 industrial robot arm. The novel arm provides the ability to regrasp the needle while the ABB robot completes all of the motion. The needle is a CT-1 needle manufactured by Ethicon Inc. The needle is a 1/2 circle taper point which has a measured radius of about 12.7 mm. The phantom tissue is manufactured by Simulab Corp. as a surgical training aid. The particular model in the experiment is a SCS-10 subcuticular tissue simulator. The advantage to using the tissue phantom is that it is homogenous and should produce repeatable results as previously shown in [6]. The purpose of using a homogenous tissue phantom is to ensure that driving the needle through the tissue in new, unpunctured, locations will produce results that depend on the type of needle drive and not the location of the needle drive.

TABLE II: Measured Forces And Torques

| Drive | $\|\bar{\boldsymbol{f}}\|$ | $\|\boldsymbol{f}\|_{\max}$ | $\|\bar{\boldsymbol{\tau}}\|$ | $\|\boldsymbol{\tau}\|_{\max}$ |
|---|---|---|---|---|
| A | 0.45 N | 1.37 N | 13.90 N-mm | 61.44 N-mm |
| B | 0.41 N | 1.16 N | 16.11 N-mm | 47.02 N-mm |

An embedded ATI nano17 force torque sensor is used to measure the wrench sensed by the gripper. The readings were sampled using a desktop computer running xPC target (designed by Mathworks® Inc.) at a 2 KHz sampling frequency. During post processing, the data was filtered using a butterworth bandpass filter (100 Hz and 5th order). This helped to remove any noise associated with the sensor.

The needle drive is performed open loop with no sensors, visual or otherwise, that helped to guide the grasper to the needle. Since the drive was open loop, minor tweaks (i.e. moving the robot regrasping point) to the needle drive had to be made to ensure that the regrasp step was successful.

### *A. Needle Drive Results*

The holonomic needle drive is shown as a stop motion sequence in Fig. 7. The gripper successfully drives and extracts the needle. Once this process is done. The gripper is then ready to begin tying the suture knot. During the needle insertion, shown in Fig. 7, it appears that the body of the gripper would interfere with the tissue during the suture. This is due to the presence of the ATI F/T sensor and will not be an issue with an actual robotic surgical system, such as the daVinci® or the Raven system [8]. Due to the size of the tissue and the placement of the gripper, only the gripper tip touched the tissue during the experiment. The non holonomic needle drive is shown as a stop motion sequence in Fig. 8. The results are visually similar to the holonomic needle drive, however, it appears that the needle is much deeper inside the tissue after the non holonomic needle drive as opposed to the holonomic drive. This is most apparent in Fig. 7:6 and 8:6. Since the optimal tissue depth of the needle is approximately the needle radius, the non holonomic needle drive reaches a more appropriate tissue depth.

## V. Results and Discussion

A plot of the force magnitudes sensed by the needle for both holonomic and non holonomic drives are shown in Fig. 9a and 9b respectively. Due to space limitations in the paper, the resulting torque magnitudes are not shown, but they have a similar shape. No attempt was made to remove the weight of the gripper and needle in the recorded plots. Each plot is broken up into distinct sections. Each section corresponds to a stage of the needle drive. The stages include, driving the needle, regrasping the needle, and finally extracting the

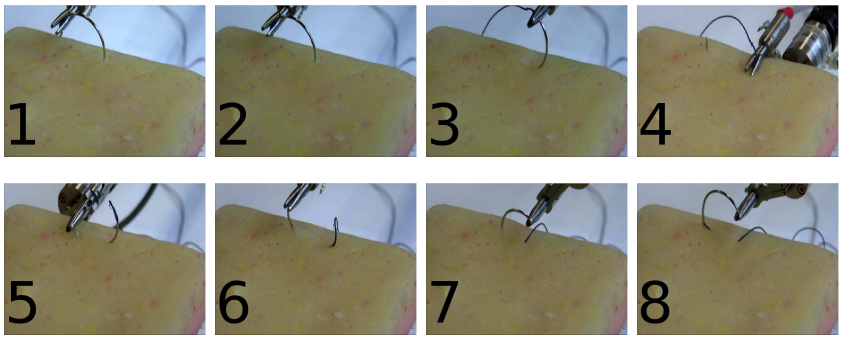


Fig. 7: Shown above is a sample group of images for driving a suture needle holonomically. The tip of the gripper that actually holds the needle is touching the tissue right before the holder regrasps the needle.

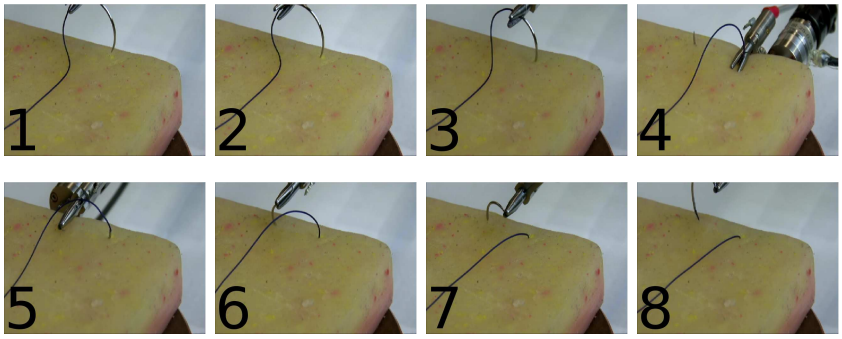


Fig. 8: Shown above is a sample group of images for driving a suture needle with the non holonomic constraint. The tip of the gripper that actually holds the needle is touching the tissue right before the holder regrasps the needle.

needle. While both sets of results have a similar overall shape, the peak forces are smaller for the non holonomic needle drive at the point right before the regrasp process starts. As shown in both Fig. 7 and Fig. 8, right before the regrasp, the gripper tip touches the tissue. While it is true that the contact will increase needle tissue forces, surgeons will often use forceps to manipulate the tissue during a suture. For that reason, the gripper contact is considered to be part of the needle drive, any forces due to such contact are therefore important components of the forces being measured. After the regrasp is completed, the non holonomic needle drive experiences a larger overall force. This is likely due to the open loop regrasp. Since the regrasp is open loop, there are small errors in the needle regrasp because of uncertainties in the needle position estimate. As a result extra forces due to positioning errors may be present.

The forces and torques of the two methods are compared using both the maximum and the mean values in Table II. The non holonomic drive (drive B) is better than the holonomic drive (drive A) in three of the four categories.

Based on the available surgical guides [11], the non holonomic needle drive appears to be better. The overall force is reduced and the needle is deeper in the tissue sample. To verify that the non holonomic drive is better, the experiment should be repeated, and the effects caused by gripper tissue contact should be investigated.

## VI. Conclusion and Future Work

The open loop needle drive experiments gave many insights into the forces and torques generated during a suture. This completes a preliminary but important step towards automated suture needle driving. In order to improve upon the current capabilities of MIS, the suture must be performed autonomously at a speed that is faster than what surgeons are able to do [12]. This can be accomplished by completing a preplanned motion with visual servoing so that during the needle regrasp, the gripper can quickly and precisely grab the needle to complete the suture. During procedures, sensor feedback (both visual and tactile) will be used to interrupt, or tweak the suturing operation if a complication arises.

The suturing technique analyzed in this study is the, simple interrupted suture. Analysis of variations of the simple interrupted suture (e.g., tissue eversion) or other suturing techniques (e.g., matress suture, continuous suture, etc. [11]) is outside the scope of this study, and will be the subject of future studies.

## References

[1] N. Abolhassani, R. Patel, and M. Moallem, "Needle insertion into soft tissue: A survey," *Medical Engineering & Physics*, vol. 29, no. 4, pp. 413 – 431, 2007. [Online]. Available: http://www.sciencedirect.com/science/article/pii/S1350453306001457

[2] R. Alterovitz, K. Goldberg, and A. Okamura, "Planning for steerable bevel-tip needle insertion through 2d soft tissue with obstacles," in *Robotics and Automation, 2005. ICRA 2005. Proceedings of the 2005 IEEE International Conference on*, april 2005, pp. 1640 – 1645.

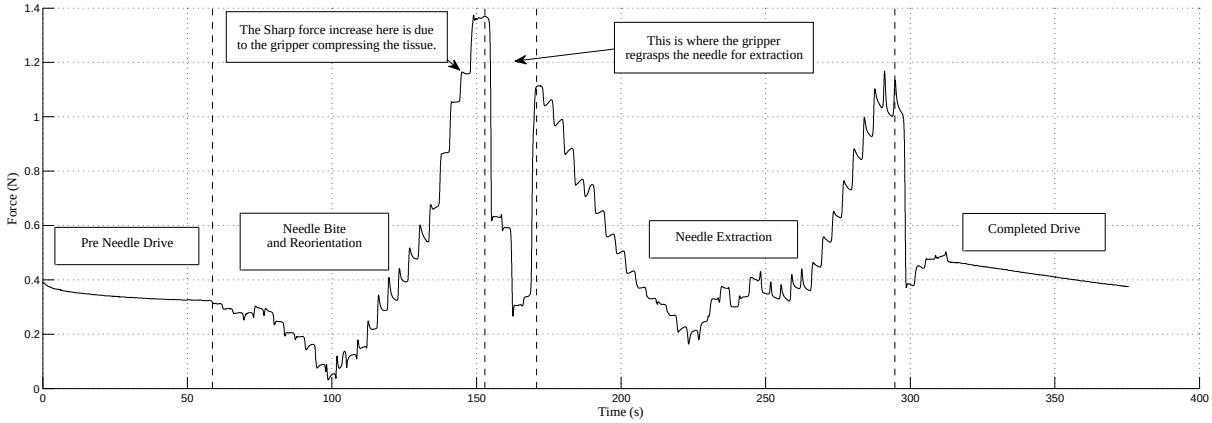


(a) Force Magnitude for the Holonomic Motion

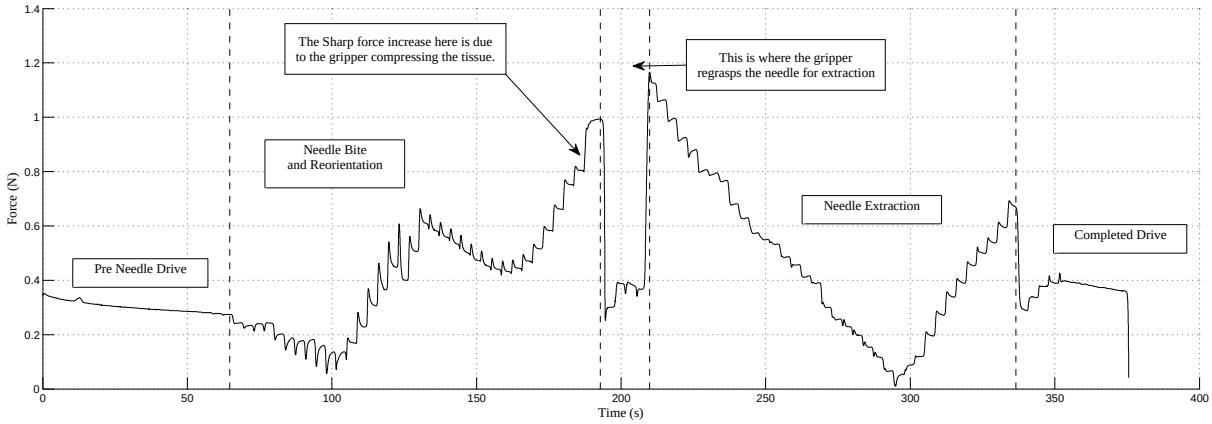


(b) Force Magnitude for the Non Holonomic motion

Fig. 9: Measured force magnitudes for both the holonomic (9a) and non holonomic (9b) needle reorientation. The sensed readings are not adjusted to remove any forces due to the weight of the needle gripper.


[3] R. Alterovitz, K. Goldberg, J. Pouliot, and I.-C. Hsu, "Sensorless motion planning for medical needle insertion in deformable tissues," *Information Technology in Biomedicine, IEEE Transactions on*, vol. 13, no. 2, pp. 217 –225, march 2009.

[4] P. I. Corke, "Visual control of robot manipulators – a review," in *Visual Servoing*. World Scientific, 1994, pp. 1–31.

[5] S. DiMaio and S. Salcudean, "Needle steering and motion planning in soft tissues," *Biomedical Engineering, IEEE Transactions on*, vol. 52, no. 6, pp. 965 –974, june 2005.

[6] R. Jackson and M. Cavusoglu, "Modeling of needle-tissue interaction forces during surgical suturing," in *Robotics and Automation (ICRA), 2012 IEEE International Conference on*, may 2012, pp. 4675 –4680.

[7] T. Liu, "Design and Prototyping of a Three Degrees of Freedom Robotic Wrist Mechanism for a Robitic Surgery System," Master's thesis, Case Western Reserve University, Cleveland, OH, 2010.

[8] M. J. H. Lum, D. C. W. Friedman, G. Sankaranarayanan, H. King, K. Fodero, R. Leuschke, B. Hannaford, J. Rosen, and M. N. Sinanan, "The raven: Design and validation of a telesurgery system," *Int. J. Rob. Res.*, vol. 28, no. 9, pp. 1183–1197, Sep. 2009. [Online]. Available: http://dx.doi.org/10.1177/0278364909101795

[9] F. Nageotte, P. Zanne, C. Doignon, and M. de Mathelin, "Stitching planning in laparoscopic surgery: Towards robot-assisted suturing." *I. J. Robotic Res.*, vol. 28, no. 10, pp. 1303–1321, 2009. [Online]. Available: http://dblp.uni-trier.de/db/journals/ijrr/ijrr28.htmlNageotteZDM09

[10] N. Semer, *Practical plastic surgery for nonsurgeons*. Hanley & Belfus, 2001. [Online]. Available: http://practicalplasticsurgery.org/

[11] D. A. Sherris and E. B. Kern, *Essential Surgical Skills*, 2nd ed. Saunders, 2004.

[12] F. Tendick, R. W. Jennings, G. K. Tharp, and L. W. Stark, "Sensing and manipulation problems in endoscopic surgery: Experiment, analysis, and observation," *Presence*, pp. 66–81, 1993.